

A magnetic phase diagram for nanoscale epitaxial BiFeO3 films

D. Sando, Florian Appert, Bin Xu, O. H C Paull, S. R Burns, C. Carretero, B. Dupé, V. Garcia, Y. Gallais, A. Sacuto, et al.

▶ **To cite this version:**

D. Sando, Florian Appert, Bin Xu, O. H C Paull, S. R Burns, et al.. A magnetic phase diagram for nanoscale epitaxial BiFeO3 films. Applied Physics Reviews, 2019, 6 (4), pp.041404. 10.1063/1.5113530 . hal-02362696

HAL Id: hal-02362696

https://normandie-univ.hal.science/hal-02362696

Submitted on 14 Nov 2019

HAL is a multi-disciplinary open access archive for the deposit and dissemination of scientific research documents, whether they are published or not. The documents may come from teaching and research institutions in France or abroad, or from public or private research centers.

L'archive ouverte pluridisciplinaire **HAL**, est destinée au dépôt et à la diffusion de documents scientifiques de niveau recherche, publiés ou non, émanant des établissements d'enseignement et de recherche français ou étrangers, des laboratoires publics ou privés.

Applied Physics Reviews ACCEPTED MANUSCRIPT

This is the author's peer reviewed, accepted manuscript. However, the online version of record will be different from this version once it has been copyedited and typeset.

PLEASE CITE THIS ARTICLE AS DOI: 10.1063/1.5113530

A Magnetic Phase Diagram for Nanoscale Epitaxial $BiFeO_3$ Films

D. Sando,[1*] F. Appert,[2] Bin Xu,[3,4] O. H. C. Paull,[1] S. R. Burns,[1] C. Carrétéro,[5] B. Dupé,[6] V. Garcia,[5] Y. Gallais,[7] A. Sacuto,[7] M. Cazayous,[7] B. Dkhil,[8] J. M. Le Breton,[2] A. Barthélémy,[5] M. Bibes,[5] L. Bellaiche,[3] V. Nagarajan,[1] and J. Juraszek[2*]

[1]School of Materials Science and Engineering, UNSW Sydney, Kensington 2052, Australia

[2]Normandie Univ., UNIROUEN, INSA Rouen, CNRS, GPM, 76000 Rouen, France

[3]Department of Physics and Institute for Nanoscience and Engineering, University of Arkansas, Fayetteville, AR 72701, USA

[4]School of Physical Science and Technology, Soochow University, Suzhou 215006, China

[5]Unité Mixte de Physique, CNRS, Thales, Univ. Paris-Sud, Université Paris-Saclay, 91767 Palaiseau, France

[6]Institute of Physics, INSPIRE Group, Johannes Gutenberg-University Mainz, 55128 Mainz, Germany

[7]Laboratoire Matériaux et Phénomènes Quantiques (UMR 7162 CNRS), Université Paris Diderot-Paris 7, 75205 Paris Cedex 13, France

[8]Laboratoire Structures, Propriétés et Modélisation des Solides, CentraleSupélec, CNRS-UMR8580, Université Paris-Saclay, 91190 Gif-sur-Yvette, France

daniel.sando@unsw.edu.au

jean.juraszek@univ-rouen.fr

Abstract:

$BiFeO_3$ thin films have attracted considerable attention by virtue of their potential application in low-energy spintronic and magnonic devices. $BiFeO_3$ possesses an intricate magnetic structure, characterized by a spin cycloid with period ~62 nm that governs the functional magnonic response, and which can be modulated or even destroyed by strain, magnetic and electric fields, or chemical doping. Literature on (110)-oriented $BiFeO_3$ films is not explicit in defining the conditions under which this cycloid persists, as its presence depends on synthesis method and thin film boundary conditions, especially in the sub-100 nm thickness regime. This report aims to end 'trial and error' approaches in determining the conditions under which this cycloid and its associated functional magnonic response exist. We show that in specific crystallographic orientations of epitaxial $BiFeO_3$, an unexplored strain parameter – the distortion in the *ab* plane of the monoclinic unit cell – significantly influences the spin structure. Combining Mössbauer spectroscopy and low energy Raman spectroscopy with first-principles-based effective Hamiltonian calculations, we show that both average strain and this distortion destroy the cycloid. For films grown on (110) oriented $SrTiO_3$ substrates, if the $BiFeO_3$ lattice parameters *a* and *b* differ by more than about 1.2 %, the cycloid is destabilized, resulting in a pseudo-collinear magnetic order ground state. We are thereby able to construct a phase diagram of the spin structure for nanoscale epitaxial $BiFeO_3$ films which aims to resolve long-standing literature inconsistencies and provides powerful guidelines for the design of future magnonic and spintronic devices.

AIP Publishing

Applied Physics Reviews ACCEPTED MANUSCRIPT
This is the author's peer reviewed, accepted manuscript. However, the online version of record will be different from this version once it has been copyedited and typeset.
PLEASE CITE THIS ARTICLE AS DOI: 10.1063/1.5113530
AIP Publishing

Bismuth ferrite ($BiFeO_3$ – BFO) is a room temperature multiferroic that has captivated researchers for the past two decades [1]. Multiferroics are widely studied since they offer great promise in memory and spintronic devices [2–4]. BFO, in addition to its multiferroic – ferroelectric and antiferromagnetic (AFM) – character, also offers appealing properties such as conductive domain walls [5,6], significant photovoltaic [7], photostriction and photonic response [8–12], as well as promise in tunnel junction, memristors, and solid state synapse applications [13–15].

The magnetic structure of BFO is rather intricate [1,16]. Below the Néel temperature ($T_N \approx 640$ K), the Fe^{3+} spins are arranged in a G-type antiferromagnetic configuration, upon which is superimposed an incommensurate cycloidal modulation of period ≈ 620 Å (Ref. [17]). In the bulk, the cycloid propagation vector is (typically) confined by symmetry to one of the degenerate directions orthogonal to the three-fold symmetry axis (that is, the direction of the polarization). Therefore, there are usually three possible propagation directions: k_1 // $[\bar{1}10]$, k_2 // $[01\bar{1}]$, and k_3 // $[10\bar{1}]$ (in pseudocubic (pc) notation). The magnetic order of BFO, particularly the existence of the cycloid, can be altered by external stimuli such as strain [4,18], magnetic [19,20] and electric [21] fields, and chemical doping/substitution [22,23]. Presently BFO research is heavily focused on the electric-field control of magnetism. In this endeavor, the most common approaches include using the exchange coupling to a ferromagnetic overlayer [24,25], controlling the weak ferromagnetic moment [26], or switching the cycloid plane with electric field [27,28]. On the other hand, a more recent development in the BFO story is the presence of magnon modes which arise from the existence of the cycloid. These spin wave excitations could be harnessed in magnonic devices [29,30] where they could be used to process information. The magnon modes in BFO can be probed with Raman spectroscopy [31,32] and are responsive to electric field [21], the latter opening the way toward low-energy magnetic or magnonic devices that are controlled by electric (rather than magnetic) stimulus.

The most promising route toward the integration of BFO in such magnonic devices is through epitaxial thin films [3]. This is because thin films offer a degree of control over crystallographic orientation, strain, and defect chemistry [33] that bulk single crystals cannot offer. For instance, in colossal magnetoresistance manganites, epitaxial strain brings about rich phase diagrams [34,35]. The spin structure in (001)-oriented BFO films has been studied by neutron diffraction, Mössbauer spectroscopy, x-ray, and real-space techniques [18,28,36–38]. In thin films, strain induces additional magnetic anisotropy which favors certain cycloid propagation vector(s). For instance, compressively strained (001)-oriented films typically show the k_1 propagation direction [18,28,37], while under tensile strain, either a cycloid with an out-of-plane propagation direction (k_2 or k_3), or even a different type of modulated spin structure, called the 'type-2 cycloid' [18], has been detected. This cycloid has a propagation direction k_4 // $[11\bar{2}]$ and spin rotation plane of $(\bar{1}10)$, both of which are different from what is observed in bulk BFO (Ref. [39]). That said, recent real-space techniques have shown that under tensile strain, either the type-2, or type-1 cycloid (or combinations thereof) can be observed. It thus appears that the most stable cycloid configuration is sensitive to more subtle effects

Applied Physics Reviews ACCEPTED MANUSCRIPT
This is the author's peer reviewed, accepted manuscript. However, the online version of record will be different from this version once it has been copyedited and typeset.
PLEASE CITE THIS ARTICLE AS DOI: 10.1063/1.5113530

such as domain structure, precise strain values, local distortion or domain populations, etc. Therefore, it is imperative to find reliable route that brings about a clear, unambiguous cycloid propagation direction.

In this context, BFO films grown in the (110) crystallographic orientation are attractive. This is because the typically eight ferroelectric (FE) polarization variants observed in (001) BFO are reduced to four in (110) BFO (Ref. [40]), and careful control of substrate and growth conditions can reduce these variants to one [5,41]. Since the FE direction and cycloid propagation vectors are linked [27], the presence of a single ferroelectric domain *removes ambiguity in the cycloid propagation direction*.

Literature on (110)-oriented BFO thin films thus far is not explicit in defining the conditions under which the cycloid persists. Specifically, the presence of the cycloid depends on synthesis conditions, as well as the thin film boundary conditions. There exists also sample-to-sample variability which complicates a universal approach to understanding the conditions for cycloid stability. Such effects appear to be more pronounced in the sub-100 nm thickness regime. For instance, the cycloid was detected in 50 nm thick films by Burns *et al*. [41], while a film of the same thickness studied by Bertinshaw *et al*. did not show this cycloidal modulation [42]. Such an observation highlights that the implementation of nanoscale BFO films in functional devices would require a 'trial and error' approach to determining if the cycloid (and its associated functional magnonic response) exists.

Here, we attempt to end such uncertainty through study of a series of 100 % ^{57}Fe-enriched BFO (110) films using Mössbauer spectroscopy, low energy Raman spectroscopy, and first-principles-based calculations, focusing on the type-2 cycloid. We show that a critical – and until now unaccounted for – property of (110)-oriented BFO, namely the anisotropy between the *a* and *b* monoclinic lattice parameters, universally dictates the cycloid stability. Specifically, for uniaxially-strained films on STO (110), if these lattice parameters differ by more than ~1.2 %, the cycloid is destabilized, and the magnetic order becomes pseudo-collinear antiferromagnetic with the spins aligned along $[001]_{pc}$. First principles-based calculations corroborate such an observation and provide insight into why the cycloid is destabilized by distortion – the lattice anisotropy gives rise to a slightly increased polarization which favors the non-cycloidal state. These results allow us to propose the first strain-distortion-spin structure phase diagram for (110) oriented $BiFeO_3$ films. It consolidates the present observations with all prior-reported literature, and in doing so provides powerful guidelines for the design of future magnonic and spintronic devices based on BFO thin films.

Epitaxial BFO thin films ~100 % enriched in ^{57}Fe were grown by pulsed laser deposition on (110)-oriented $SrTiO_3$ (STO) substrates, as reported previously [9,18,43]. Here, we focus on a set of five films (denoted 1-5) with thickness 19-144 nm. In the (110) orientation, BFO crystallizes in a M_B monoclinic structure [**Fig. 1(a)**] (*Cm* space group with $\frac{a_{mono}}{\sqrt{2}} > c_{mono}$) [3,5,40]. The lattice parameters are a_{BFO}, b_{BFO} (// $[\bar{1}10]_{STO}$), and c_{BFO} (// $[001]_{STO}$), see **Fig. 1(a)**. Note that a_{BFO} is almost parallel to the growth axis with $(100)_{BFO}$ parallel to $(110)_{STO}$. X-ray diffraction (XRD) 2θ-ω scans and reciprocal space mapping (RSM) (see

Applied Physics Reviews ACCEPTED MANUSCRIPT
This is the author's peer reviewed, accepted manuscript. However, the online version of record will be different from this version once it has been copyedited and typeset.
PLEASE CITE THIS ARTICLE AS DOI: 10.1063/1.5113530
AIP Publishing

Supplementary Material for representative examples) evidence high-quality, single phase epitaxial films, and atomic force microscopy topography scans [**Fig. 1(b)**] confirm low surface roughness. The ferroelectric domain structure was probed by piezoresponse force microscopy (PFM) (full data not shown). A typical out-of-plane PFM phase image for the 126 nm film shows a homogeneous contrast indicating a single ferroelectric domain [**Fig. 1(b)**]. The polarization lies in a (*hhl*) plane between [110]-a_{BFO} out-of-plane and [001]-c_{BFO} in-plane directions with a direction very close to [110]-a_{BFO}. For these five films, both PFM and XRD RSM measurements showed either a single FE domain, or two domains, of which the dominant had a > 80 % phase fraction.

The lattice parameters and monoclinic angle are plotted as a function of thickness in **Fig. 1(c)** (representative XRD data used for calculating these values are given in **Section 3** of the Supplementary Material). A monotonic increase (decrease) in the in-plane b_{BFO} and c_{BFO} (out-of-plane a_{BFO}) parameters is observed, consistent with gradual strain relaxation, as reported previously [40]. Notably here, the monoclinic angle β shows negligible dependence on thickness (within experimental uncertainty). The reported magnetic structure of BFO thin films grown on (110) oriented substrates, with the lattice constants (when available) are summarized in **Table S1** (Supplementary Material). Notably, there is some variation regarding the stability of the cycloid as a function of thickness.

We define the average strain (ε) of the BFO unit cell as $\varepsilon = \frac{\sqrt{a_{\mathrm{BFO}} b_{\mathrm{BFO}}/2} - a_{bulk}}{a_{bulk}} \times 100\ \%$, where $a_{bulk} = \sqrt[3]{a_{\mathrm{BFO}} b_{\mathrm{BFO}} c_{\mathrm{BFO}}/2}$ is the effective 'bulk' pseudo-cubic lattice parameter of the film. [For simplicity the monoclinic angle β is neglected since it changes the unit cell volume by less than 0.1 %.]

Critical to this work, we define a new parameter, which we call the *distortion* (δ) of the unit cell, as $\delta = \left(\frac{a_{\mathrm{BFO}}}{b_{\mathrm{BFO}}} - 1\right) \times 100\ \%$. This distortion could be considered the BFO 'in-plane anisotropic distortion'. A similar concept has been used for T-like BFO films [4] and has been shown to influence the magnetic order in that particular phase [44]. These formulations capture in an elegant way the most important deformations in strained (110) BFO films. The values of ε and δ for the present set of films are plotted in **Fig. 1(d)** (all lattice parameters and ε and δ values for all samples are tabulated in **Table S2**, Supplementary Material). Notably, the average strain of the BFO unit cell is almost constant at ε = 0.7 %, while the distortion shows a monotonic decrease with thickness. This sample set therefore offers a unique possibility to examine the influence of the δ parameter on magnetic structure while the average strain (ε) remains virtually constant.

To probe the magnetic structure of the films, we used conversion electron Mössbauer spectroscopy (CEMS) at 295 K. This technique, well suited to thin films, probes the magnetic environment of the ^{57}Fe ions. Fitting the spectra using the procedure described in Ref. [18] allows to detect the existence of cycloidal order, as well as the average spin direction (*i.e.*, the direction of the AFM vector ***L***). Briefly, for the cases described here, an asymmetry (in breadth and height of the peaks) of the CEMS spectrum strongly suggests the

Applied Physics Reviews ACCEPTED MANUSCRIPT
This is the author's peer reviewed, accepted manuscript. However, the online version of record will be different from this version once it has been copyedited and typeset.
PLEASE CITE THIS ARTICLE AS DOI: 10.1063/1.5113530
AIP Publishing

existence of cycloidal order, while a lack of asymmetry (*i.e.*, a symmetric spectrum) suggests non-cycloidal order. Further, the intensity ratio of the 2nd and 3rd peak, denoted R_{23}, gives information about the average spin direction relative to the direction of the incoming γ-rays. In normal incidence, the R_{23} value is 4 in the case of in-plane orientation of the Fe spins, while out-of-plane spin orientation leads to $R_{23} = 0$. Such information allows us to determine the spin structure of BFO, and, importantly, discern if the film has cycloidal magnetic order or pseudo-collinear AFM.

The CEMS spectra at room temperature (**Fig. 2**) in normal incidence for all the BFO films exhibit a six-line magnetic hyperfine pattern with hyperfine parameters (isomer shift $\delta \sim 0.37$ mm/s and hyperfine field $B_{hf} \sim 49$ T) typical for Fe^{3+} ions in the rhombohedral BFO phase [45,46]. For the 19-93 nm films [**Fig. 2(a-c)**], the spectrum is symmetric and the 2nd (or 5th) peak (counted from the left) more intense than the 1st (or 6th) peak. These spectra have been fit using a collinear spin structure (symmetric sextet) and the R_{23} value deduced from the fit (R_{23} close to 4) indicates that the direction of the spins is confined to the film plane. Additional measurements with the sample tilted relative to the incoming γ-ray direction (see **Fig. S4**, Supplementary Material) confirm that the antiferromagnetic vector $\boldsymbol{L}$ is along the $[001]_{pc}$ in-plane direction.

In contrast to the thinner samples, the films of thickness 126 nm and 144 nm exhibit spectra with the 1st (or 6th) peak more intense than the 2nd (or 5th) peak along with a slight asymmetry [**Fig. 2(d-e)**]. Such an observation reflects the fact that a greater number of Fe spins are out of the film plane, *i.e.* consistent with a cycloidal modulation. The asymmetry in the spectra for the 144 nm film is shown more clearly when the spectrum is zoomed in [**Fig. 2(f)**]. It is observed that the difference in linewidth of the 1st and 6th peaks is 0.05 mm/s (± 0.012 mm/s), similar in magnitude to the difference observed for CEMS spectra for cycloidal BFO [18]. Such an observation is a hallmark of the cycloidal modulation, since a purely collinear magnetic structure would give perfectly symmetric peaks. Fitting the spectra with a model comprising a collinear component and a harmonic cycloid with spins in the $(\bar{1}10)$-plane yields approximately 40% cycloid 60 % collinear phase for both the 126 and 144 nm films; however, such an observation could also be consistent with an anharmonic cycloid [47] where a strain-induced anisotropy causes the spins to 'bunch' along the in-plane $[001]_{pc}$ direction. This partially destabilized cycloid is suggested to be the result of the moderate tensile strain experienced by the BFO film [18]. To summarize this analysis, the CEMS data suggest that for these samples, a transition from non-cycloidal to cycloidal order occurs at a thickness of ~90 nm.

What is the origin of such a transition between cycloidal and non-cycloidal order? Since previous reports have shown evidence for the cycloid in films as thin as 50 nm for (110) BFO (Ref. [41]), and 30 nm for (001) BFO (Ref. [28]), we rule out the possibility that finite size effects (*i.e.*, thinner films) affect cycloid stability and must here search for some other factor to explain the observations. For this, one needs to return to the structural data [**Fig. 1(d)**]. Strikingly, it appears that the CEMS measurements suggest that a large distortion of $\delta > 1.1$ % destabilizes the cycloid in favor of collinear AFM order with spins aligned along $[001]_{pc}$.

Applied Physics Reviews ACCEPTED MANUSCRIPT
This is the author's peer reviewed, accepted manuscript. However, the online version of record will be different from this version once it has been copyedited and typeset.
PLEASE CITE THIS ARTICLE AS DOI: 10.1063/1.5113530

To delve further into such a possibility, first-principles-based effective Hamiltonian calculations were performed to understand the influence of δ on the cycloid. Since in (110)-oriented BFO the type-2 cycloid is almost exclusively observed [18,39], our calculations consider this cycloid, along with various collinear antiferromagnetic arrangements with different spin directions. The effective Hamiltonian approach considers nearest and next-nearest neighbors [48] in the spin-current model [49–52], and in the present calculations the spin-current parameters C_1 and C_2 were chosen to reproduce the δ dependence of the magnetic ground state at 0.7 % strain. In the simulations, the value of strain (taken from experiment for the typical strain values when BFO is grown on STO substrate) was fixed at ε = +0.7 %, and the distortion δ was systematically swept between 0 and 1.5 %. The total energy of the type-2 cycloid relative to the collinear AFM phase with $\boldsymbol{L}$ // $[001]_{pc}$ is plotted as a function of distortion δ in **Fig. 3(a)** (the full data can be found in **Section 7** of the Supplementary Material).

The calculations show that for values of δ greater than ≈ 1.2 %, the type-2 cycloid becomes less energetically favorable than the collinear AFM state (The full calculation details considering other collinear states is shown in **Fig. S6**, Supplementary Material). Such a spin structure is consistent with previous observations on (001)-oriented M_B monoclinic BFO films with ε = +0.9 %, where the spin direction was found to be close to $[001]_{pc}$ (Ref. [53]). For values of δ less than ≈ 1.2 % on the other hand, the type 2 cycloid, with propagation vector along $[11\bar{2}]$, is energetically favorable. These calculations thus show that in BFO, it is not only the average strain ε (Ref. [18]), but also the distortion δ that defines the magnetic ground structure.

With such observations in mind, we are now uniquely poised to rationalize all published data in the literature. **Figure 4** shows the proposed phase diagram for (110)-oriented BFO films, as a function of the average strain ε and the distortion δ. Reported literature data [39,41,42,53] are denoted by squares, while the data from the present study are shown as circles. The boundary between cycloidal and non-cycloidal order plotted in **Fig. 4** is estimated and is consistent with further calculations (see Supplementary Material) that indicate that larger values of strain bring the transition between AFM and cycloidal orders to lower values of distortion.

The phase diagram shows that for lower values of average strain, the cycloid is more resistant to larger values of distortion δ, while for larger ~1.2 % of average strain the cycloid is unstable for much lower values of δ. We can rationalize such an observation with the theory (full details are given in **Section 7** of the Supplementary Material). Lower values of average strain are numerically found to yield smaller polarization, which stabilizes the cycloid over the non-cycloidal configurations. Such a relationship between polarization and magnetic structure is consistent with the fact that the cycloid in BFO is known to be destroyed with sufficient electric field or strain, factors that enhance the overall polarization [21,54].

To expand our exploration of the phase diagram in **Fig. 4**, we grew two further BFO films on (110)-oriented $(LaAlO_3)_{0.3}(Sr_2TaAlO_6)_{0.7}$ (LSAT). Since LSAT has a smaller lattice parameter (a_{LSAT} = 3.868 Å) than STO, this substrate imposes a larger value of ε (up to 1.1 %) with δ between 0.5 and 0.7 %. We used low-

Applied Physics Reviews ACCEPTED MANUSCRIPT
This is the author's peer reviewed, accepted manuscript. However, the online version of record will be different from this version once it has been copyedited and typeset.
PLEASE CITE THIS ARTICLE AS DOI: 10.1063/1.5113530

energy Raman spectroscopy [18,31] to detect the presence of the cycloid in these samples. The full details are found in **Section 6** of the Supplementary Material. In summary here, we find that according to the Raman spectra, both samples possess at least one cycloid – thus implying that even at values of $\varepsilon = 1.1$ %, the cycloid is not destabilized, *provided that the level of distortion is sufficiently low* (i.e., $\delta \leq 0.7$ %). Such an observation would suggest that, in contrast with (001) films where the average strain ε plays a decisive role [18], the distortion δ is likely the key structural parameter in (110) oriented BFO films.

Finally, the paper concludes with an assessment of the proposed phase diagram. In addition to the seven samples studied earlier, a further four samples (denoted A, B, C, D) were considered. The additional samples (thickness 15-200 nm) were once again prepared by PLD on (110)-oriented STO. Since the structure of BFO films can be affected by the type of ablation laser used for growth [8], the additional samples were grown using a frequency-tripled Nd:YAG laser (as for the original five samples), and also by excimer laser (as for Samples R1 and R2) [28]. For each sample, XRD was used to measure the lattice constants, the values of (ε, δ) were determined using XRD by the method described above, and the spin structure predicted from the phase diagram of **Fig. 4**. The four samples were then measured by CEMS. The samples were randomized (with a further six samples used in a separate study to be published elsewhere) and labelled arbitrarily (a *double-blind* test) to ensure no bias was introduced during the fitting of the CEMS spectra. The results of this test are included in the phase diagram of **Fig. 4**. Notably, Sample A (t = 200 nm; $\varepsilon = 0.5$ %; $\delta = 0.87$ %) and Sample C were successfully predicted and identified to have cycloidal order, while samples B and D were found to have a minor contribution from cycloidal order (< 30 %), which we label as collinear AFM order in **Fig. 4** (full details in Supplementary Material). This test thus demonstrates that extrinsic influences such as growth chamber (including ablation laser type) play less pivotal roles than the values of (ε, δ) to predict the magnetic order in (110)-oriented BFO films.

In summary, we have proposed a phase diagram for the spin structure in (110)-oriented BFO. Combining Mössbauer spectroscopy, Raman spectroscopy, and first principles-based calculations, we showed that not only the average strain, but the *distortion* of BFO (the difference in a and b lattice parameters of the monoclinic unit cell) plays a critical role in the cycloid's stability. For BFO on STO (110), if the lattice parameters a and b differ by more than 1.2 % the cycloid is destabilized in favor of a collinear AFM order with the antiferromagnetic vector $\boldsymbol{L}$ aligned along the $[001]_{pc}$ direction. On the other hand, for distortion values less than about 1.2 %, the type-2 cycloid, with spin rotation plane $(\bar{1}10)$, is found to be stable. This effect is found, through analysis in the effective Hamiltonian framework, to be related to the modification of polarization caused by the distortion, and in turn the interplay between electric dipoles and magnetic moments. Interestingly, low-energy Raman spectroscopy measurements on films with higher values of strain indicate that the average strain is less critical than the value of distortion. Finally, a double-blind test was performed, to assess the validity of the proposed phase diagram. The spin structures were predicted based on the lattice parameters and were in reasonable agreement with the results of CEMS measurements, thus attesting to the validity of the phase diagram. The results presented here show that more subtle strain

Applied Physics Reviews ACCEPTED MANUSCRIPT

This is the author's peer reviewed, accepted manuscript. However, the online version of record will be different from this version once it has been copyedited and typeset.

PLEASE CITE THIS ARTICLE AS DOI: 10.1063/1.5113530

parameters play a significant role in the magnetic ground state of BFO and set clear guidelines for the engineering of BFO films for future magnonic and spintronic devices.

AIP Publishing

Applied Physics Reviews ACCEPTED MANUSCRIPT

This is the author's peer reviewed, accepted manuscript. However, the online version of record will be different from this version once it has been copyedited and typeset.

PLEASE CITE THIS ARTICLE AS DOI: 10.1063/1.5113530

Figure Captions:

Figure 1. Sample structural details: (a) Schematic of the monoclinic M_B unit cell as found in (110)-oriented films (adapted from Ref. [40]). In such a monoclinic structure, the a_{BFO} lattice parameter is in fact out of plane; *i.e.* close to parallel with the [110] STO direction. (b) (i) atomic force microscopy (AFM) topography image of the 126 nm film showing root-mean-square (rms) roughness of 0.4 nm. (b) (ii) PFM out-of-plane phase image, showing a single FE domain for the 126 nm film. (c) lattice parameters and monoclinic angle as a function of thickness; a monotonic increase (decrease) in the in-plane b_{BFO} and c_{BFO} (out-of-plane a_{BFO}) parameters is observed, consistent with gradual strain relaxation. The values of strain (ε) and distortion (δ) for the present set of films shown here.

Figure 2. Conversion electron Mössbauer spectra of (110) $BiFeO_3$ films with thickness 19-144 nm (Samples 1-5). For films 19-93 nm in thickness (a-c), the spectra are symmetric with R_{23} ~ 4, indicating no cycloid and spins confined in the film plane. (d) The 93 nm film shows an almost perfectly symmetric spectrum. (e-f) the 126 and 144 nm films show slightly asymmetric spectra and can be fit with a model comprising a mixture of cycloidal and collinear spin structures. (g) The linewidth of peaks 1 and 6 for the 144 nm film is significantly different, consistent with a cycloid modulation. For all spectra, the error for the experimental data is smaller than the symbol size.

Figure 3. First principles-based calculations. (a) Total energy of the type-2 cycloid relative to the collinear AFM phase with $\boldsymbol{L}$ // $[001]_{pc}$, in (110) BFO films (with ε = +0.7 %) as a function of unit cell distortion δ. For δ < 1.2 %, the type-2 cycloid with k_4 // $[11\bar{2}]$ propagation direction is found to be the ground state, while if δ ≥ 1.2 %, a collinear AFM order with spins aligned along [001] is stable. Depictions of (b) the type-2 cycloid (rotations are 8× exaggerated) and (c) collinear AFM order with $\boldsymbol{L}$ // [001], respectively, for six monoclinic BFO unit cells.

Figure 4. Proposed phase diagram for (110)-oriented BFO films as a function of the average strain ε and distortion δ. Herein, we report literature data (Refs. [39,41,42,53]) by square symbols, and by circles the data from the present study. Regions where the cycloid is detected are shaded in orange, while the blue areas are parameters of distortion and strain where cycloid is not stable. The phase boundary (pale green) is estimated based on spread of the experimental results. It is visible that for lower values of average strain the cycloid appears to be more resistant to larger values of δ, while for larger (~1.2 %) average strain the cycloid becomes destabilized for much lower values of δ.

AIP Publishing

Applied Physics Reviews ACCEPTED MANUSCRIPT

This is the author's peer reviewed, accepted manuscript. However, the online version of record will be different from this version once it has been copyedited and typeset.
PLEASE CITE THIS ARTICLE AS DOI: 10.1063/1.5113530

Acknowledgements

D.S. acknowledges the support of an Australian Nanotechnology Network (ANN) travel fellowship. This research was partially supported by the Australian Research Council Centre of Excellence in Future Low-Energy Electronics Technologies (Project number CE170100039), and the Australian Research Council (ARC) through the funding of Discovery Grants and funded by the Australian Government. O.H.C.P. and S.R.B would like to thank AINSE Limited for providing financial assistance (Award - PGRA) to enable this work. We thank S. Fusil for fruitful discussions. Funding of this work by Region of Normandy (France) and the European Regional Development Fund of Normandy (ERDF) in the frame of the MAGMA project is acknowledged. We thank support from the French Agence Nationale de la Recherche (ANR) through projects EXPAND and PIAF. This work is supported by a public grant overseen by the French National Research Agency (ANR) as part of the 'Investissements d'Avenir' program (Labex NanoSaclay, reference: ANR-10-LABX-0035). B.X. thanks the financial support of the Department of Energy, Office of Basic Energy Sciences, under Contract ER-46612 and the support from Priority Academic Program Development (PAPD) of Jiangsu Higher Education Institutions. L.B. and V.N. thank DARPA Grant No. HR0011727183-D18AP00010 (TEE Program).

Supplementary Material

See Supplementary Material for 1) Survey of literature for (110)-oriented $BiFeO_3$ films; 2) Summary of samples used in the present work; 3) Structural characterization of (110)-oriented $BiFeO_3$ films; 4) Experimental details for Conversion Electron Mössbauer Spectrometry (CEMS), and fitting for mixed cycloid/collinear phases in BFO//STO (110); 5) CEMS measurements in tilted geometries; 6) Low-energy Raman spectroscopy; and 7) Additional computational details regarding the effect of ε and δ on the magnetic ground state.

AIP Publishing

Applied Physics Reviews ACCEPTED MANUSCRIPT

This is the author's peer reviewed, accepted manuscript. However, the online version of record will be different from this version once it has been copyedited and typeset.

PLEASE CITE THIS ARTICLE AS DOI: 10.1063/1.5113530

References

[1] G. Catalan and J. F. Scott, Adv. Mater. **21**, 2463 (2009).

[2] M. Bibes and A. Barthélémy, Nat. Mater. **7**, 425 (2008).

[3] D. Sando, A. Barthélémy, and M. Bibes, J. Phys. Condens. Matter **26**, 473201 (2014).

[4] D. Sando, B. Xu, L. Bellaiche, and V. Nagarajan, Appl. Phys. Rev. **3**, 011106 (2016).

[5] P. Sharma, Q. Zhang, D. Sando, C. H. Lei, Y. Liu, J. Li, V. Nagarajan, and J. Seidel, Sci. Adv. **3**, e1700512 (2017).

[6] T. Young, P. Sharma, D. H. Kim, T. D. Ha, J.-Y. Juang, Y.-H. Chu, J. Seidel, V. Nagarajan, S. Yasui, M. Itoh, and D. Sando, APL Mater. **6**, 026102 (2018).

[7] T. Choi, S. Lee, Y. J. Choi, V. Kiryukhin, and S.-W. Cheong, Science. **324**, 63 (2009).

[8] D. Sando, C. Carrétéro, M. N. Grisolia, A. Barthélémy, V. Nagarajan, and M. Bibes, Adv. Opt. Mater. **6**, 1700836 (2017).

[9] D. Sando, P. Hermet, J. Allibe, J. Bourderionnet, S. Fusil, C. Carrétéro, E. Jacquet, J.-C. Mage, D. Dolfi, A. Barthélémy, P. Ghosez, and M. Bibes, Phys. Rev. B **89**, 195106 (2014).

[10] D. Sando, Y. Yang, C. Paillard, B. Dkhil, L. Bellaiche, and V. Nagarajan, Appl. Phys. Rev. **5**, 041108 (2018).

[11] C. Paillard, B. Xu, B. Dkhil, G. Geneste, and L. Bellaiche, Phys. Rev. Lett. **116**, 247401 (2016).

[12] M. Lejman, G. Vaudel, I. C. Infante, P. Gemeiner, V. E. Gusev, B. Dkhil, and P. Ruello, Nat. Commun. **5**, 4301 (2014).

[13] V. Garcia and M. Bibes, Nat. Commun. **5**, 4289 (2014).

[14] S. Boyn, A. M. Douglas, C. Blouzon, P. Turner, A. Barthélémy, M. Bibes, S. Fusil, J. M. Gregg, and V. Garcia, Appl. Phys. Lett. **109**, 1 (2016).

[15] S. Boyn, J. Grollier, G. Lecerf, B. Xu, N. Locatelli, S. Fusil, S. Girod, C. Carrétéro, K. Garcia, S. Xavier, J. Tomas, L. Bellaiche, M. Bibes, A. Barthélémy, S. Saighi, and V. Garcia, Nat. Commun. **8**, 14736 (2017).

[16] J.-G. Park, M. D. Le, J. Jeong, and S. Lee, J. Phys. Condens. Matter **26**, 433202 (2014).

[17] I. Sosnowska, T. Peterlin-Neumaier, and E. Steichele, J. Phys. C Solid State Phys. **15**, 4835 (1982).

AIP Publishing

Applied Physics Reviews ACCEPTED MANUSCRIPT
This is the author's peer reviewed, accepted manuscript. However, the online version of record will be different from this version once it has been copyedited and typeset.
PLEASE CITE THIS ARTICLE AS DOI: 10.1063/1.5113530

[18] D. Sando, A. Agbelele, D. Rahmedov, J. Liu, P. Rovillain, C. Toulouse, I. C. Infante, A. P. Pyatakov, S. Fusil, E. Jacquet, C. Carrétéro, C. Deranlot, S. Lisenkov, D. Wang, J.-M. M. Le Breton, M. Cazayous, A. Sacuto, J. Juraszek, A. K. Zvezdin, L. Bellaiche, B. Dkhil, A. Barthélémy, and M. Bibes, Nat. Mater. **12**, 641 (2013).

[19] B. Ruette, S. Zvyagin, A. P. Pyatakov, A. Bush, J. F. Li, V. I. Belotelov, A. K. Zvezdin, and D. Viehland, Phys. Rev. B **69**, 064114 (2004).

[20] A. Agbelele, D. Sando, C. Toulouse, C. Paillard, R. D. Johnson, R. Rüffer, A. F. Popkov, C. Carrétéro, P. Rovillain, J.-M. Le Breton, B. Dkhil, M. Cazayous, Y. Gallais, M.-A. Méasson, A. Sacuto, P. Manuel, A. K. Zvezdin, A. Barthélémy, J. Juraszek, and M. Bibes, Adv. Mater. **29**, (2017).

[21] P. Rovillain, R. De Sousa, Y. Gallais, A. Sacuto, M. Méasson, D. Colson, A. Forget, M. Bibes, A. Barthélémy, and M. Cazayous, Nat. Mater. **9**, 975 (2010).

[22] I. Sosnowska, W. Schäfer, W. Kockelmann, K. H. Andersen, and I. O. Troyanchuk, Appl. Phys. A **74**, S1040 (2002).

[23] J. Chen, B. Xu, X. Q. Liu, T. T. Gao, L. Bellaiche, and X. M. Chen, Adv. Funct. Mater. **29**, 1 (2019).

[24] J. Allibe, S. Fusil, K. Bouzehouane, C. Daumont, D. Sando, E. Jacquet, C. Deranlot, M. Bibes, and A. Barthélémy, Nano Lett. **12**, 1141 (2012).

[25] L. W. Martin, Y.-H. Chu, M. B. Holcomb, M. Huijben, P. Yu, S. Han, D. Lee, S. X. Wang, and R. Ramesh, Nano Lett. **8**, 2050 (2008).

[26] J. T. Heron, J. L. Bosse, Q. He, Y. Gao, M. Trassin, L. Ye, J. D. Clarkson, C. Wang, J. Liu, S. Salahuddin, D. C. Ralph, D. G. Schlom, J. Íñiguez, B. D. Huey, and R. Ramesh, Nature **516**, 370 (2014).

[27] D. Lebeugle, D. Colson, A. Forget, M. Viret, A. M. Bataille, and A. Gukasov, Phys. Rev. Lett. **100**, 227602 (2008).

[28] I. Gross, W. Akhtar, V. Garcia, L. J. Martínez, S. Chouaieb, K. Garcia, C. Carrétéro, A. Barthélémy, P. Appel, P. Maletinsky, J.-V. Kim, J. Y. Chauleau, N. Jaouen, M. Viret, M. Bibes, S. Fusil, and V. Jacques, Nature **549**, 252 (2017).

[29] V. V Kruglyak, S. O. Demokritov, and D. Grundler, J. Phys. D. Appl. Phys. **43**, 264001 (2010).

[30] W. Chen and M. Sigrist, Phys. Rev. Lett. **114**, 157203 (2015).

[31] M. Cazayous, Y. Gallais, A. Sacuto, R. de Sousa, D. Lebeugle, and D. Colson, Phys. Rev. Lett. **101**, 037601 (2008).

AIP Publishing

Applied Physics Reviews ACCEPTED MANUSCRIPT
This is the author's peer reviewed, accepted manuscript. However, the online version of record will be different from this version once it has been copyedited and typeset.
PLEASE CITE THIS ARTICLE AS DOI: 10.1063/1.5113530

[32] J. Buhot, C. Toulouse, Y. Gallais, A. Sacuto, R. de Sousa, D. Wang, L. Bellaiche, M. Bibes, A. Barthélémy, A. Forget, D. Colson, M. Cazayous, and M.-A. Measson, Phys. Rev. Lett. **115**, 267204 (2015).

[33] L. R. Dedon, S. Saremi, Z. Chen, A. R. Damodaran, B. A. Apgar, R. Gao, and L. W. Martin, Chem. Mater. **28**, 5952 (2016).

[34] C. Adamo, X. Ke, H. Q. Wang, H. L. Xin, T. Heeg, M. E. Hawley, W. Zander, J. Schubert, P. Schiffer, D. A. Muller, L. Maritato, and D. G. Schlom, Appl. Phys. Lett. **95**, 112504 (2009).

[35] H. Boschker, J. Kautz, E. P. Houwman, W. Siemons, D. H. A. Blank, M. Huijben, G. Koster, A. Vailionis, and G. Rijnders, Phys. Rev. Lett. **109**, 157207 (2012).

[36] W. Saenrang, B. A. Davidson, F. Maccherozzi, J. P. Podkaminer, J. Irwin, R. D. Johnson, J. W. Freeland, J. Íñiguez, J. L. Schad, K. Reierson, J. C. Frederick, C. A. F. Vaz, L. Howald, T. H. Kim, S. Ryu, M. Veenendaal, P. G. Radaelli, S. S. Dhesi, M. S. Rzchowski, and C. B. Eom, Nat. Commun. **8**, 1583 (2017).

[37] X. Ke, P. P. Zhang, S. H. Baek, J. Zarestky, W. Tian, and C. B. Eom, Phys. Rev. B **82**, 134448 (2010).

[38] R. D. Johnson, P. Barone, A. Bombardi, R. J. Bean, S. Picozzi, P. G. Radaelli, Y. S. Oh, S.-W. Cheong, and L. C. Chapon, Phys. Rev. Lett. **110**, 217206 (2013).

[39] W. Ratcliff, D. Kan, W. Chen, S. Watson, S. Chi, R. Erwin, G. J. McIntyre, S. C. Capelli, and I. Takeuchi, Adv. Funct. Mater. **21**, 1567 (2011).

[40] D. Kan and I. Takeuchi, J. Appl. Phys. **108**, 014104 (2010).

[41] S. R. Burns, D. Sando, B. Xu, B. Dupé, L. Russell, G. Deng, R. Clements, O. H. C. Paull, J. Seidel, L. Bellaiche, N. Valanoor, and C. Ulrich, NPJ Quantum Mater. **4**, 18 (2019).

[42] J. Bertinshaw, R. Maran, S. J. Callori, V. Ramesh, J. Cheung, S. A. Danilkin, W. T. Lee, S. Hu, J. Seidel, N. Valanoor, and C. Ulrich, Nat. Commun. **7**, 12664 (2016).

[43] H. Béa, M. Bibes, A. Barthélémy, K. Bouzehouane, E. Jacquet, A. Khodan, J.-P. Contour, S. Fusil, F. Wyczisk, A. Forget, D. Lebeugle, D. Colson, and M. Viret, Appl. Phys. Lett. **87**, 72508 (2005).

[44] G. J. MacDougall, H. M. Christen, W. Siemons, M. D. Biegalski, J. L. Zarestky, S. Liang, E. Dagotto, and S. E. Nagler, Phys. Rev. B **85**, 100406(R) (2012).

[45] D. Lebeugle, D. Colson, A. Forget, M. Viret, P. Bonville, J. F. Marucco, and S. Fusil, Phys. Rev. B **76**, 024116 (2007).

AIP Publishing

Applied Physics Reviews ACCEPTED MANUSCRIPT

This is the author's peer reviewed, accepted manuscript. However, the online version of record will be different from this version once it has been copyedited and typeset.
PLEASE CITE THIS ARTICLE AS DOI: 10.1063/1.5113530

[46] D. Sando, A. Agbelele, C. Daumont, D. Rahmedov, W. Ren, I. C. Infante, S. Lisenkov, S. Prosandeev, S. Fusil, E. Jacquet, C. Carretero, S. Petit, M. Cazayous, J. Juraszek, J.-M. Le Breton, L. Bellaiche, B. Dkhil, A. Barthelemy, and M. Bibes, Philos. Trans. R. Soc. A **372**, 20120438 (2014).

[47] A. Zalesskii, A. Zvezdin, A. Frolov, and A. Bush, J. Exp. Theor. Phys. Lett. **71**, 682 (2000).

[48] B. Xu, B. Dupé, C. Xu, H. Xiang, and L. Bellaiche, Phys. Rev. B **98**, 184420 (2018).

[49] A. Raeliarijaona, S. Singh, H. Fu, and L. Bellaiche, Phys. Rev. Lett. **110**, 137205 (2013).

[50] H. Katsura, N. Nagaosa, and A. V. Balatsky, Phys. Rev. Lett. **95**, 1 (2005).

[51] D. Rahmedov, D. Wang, J. Íñiguez, and L. Bellaiche, Phys. Rev. Lett. **109**, 037207 (2012).

[52] C. Xu, B. Xu, B. Dupé, and L. Bellaiche, Phys. Rev. B **99**, 1 (2019).

[53] D. Sando, F. Appert, S. R. Burns, Q. Zhang, Y. Gallais, A. Sacuto, M. Cazayous, V. Garcia, S. Fusil, C. Carrétéro, J. M. Le Breton, A. Barthélémy, M. Bibes, J. Juraszek, and V. Nagarajan, Phys. Rev. Mater. **3**, 104404 (2019).

[54] B. Dupé, I. C. Infante, G. Geneste, P.-E. Janolin, M. Bibes, A. Barthélémy, S. Lisenkov, L. Bellaiche, S. Ravy, and B. Dkhil, Phys. Rev. B **81**, 144128 (2010).

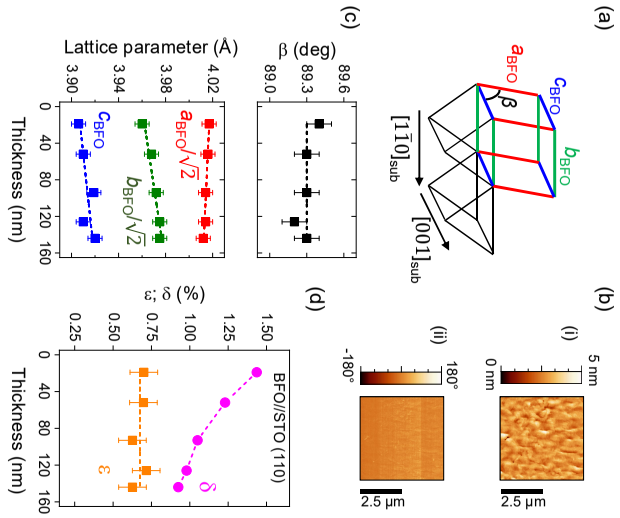
AIP Publishing

AIP Publishing

Applied Physics Reviews ACCEPTED MANUSCRIPT

This is the author's peer reviewed, accepted manuscript. However, the online version of record will be different from this version once it has been copyedited and typeset.

PLEASE CITE THIS ARTICLE AS DOI: 10.1063/1.5113530

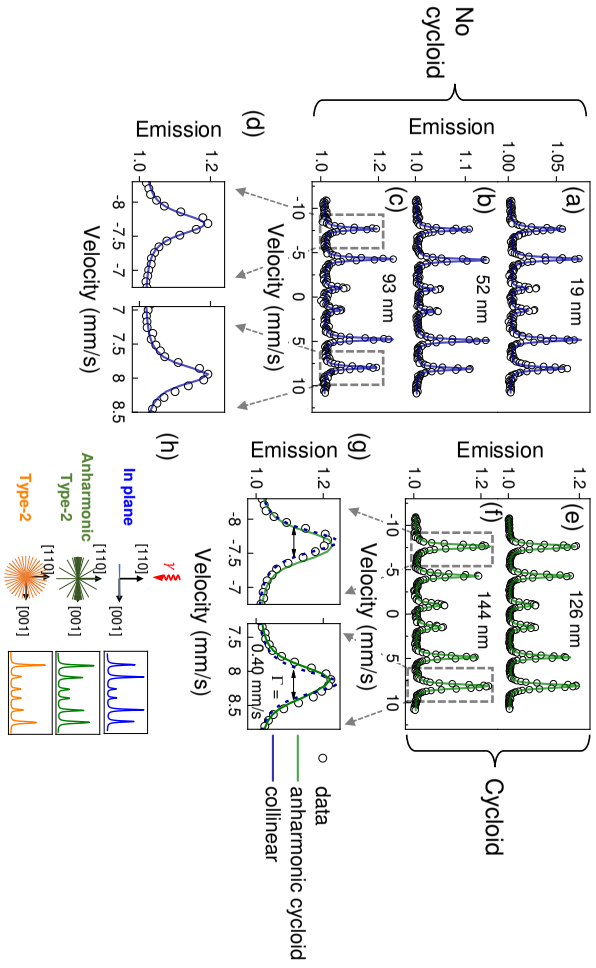


AIP Publishing

Applied Physics Reviews ACCEPTED MANUSCRIPT

This is the author's peer reviewed, accepted manuscript. However, the online version of record will be different from this version once it has been copyedited and typeset.

PLEASE CITE THIS ARTICLE AS DOI: 10.1063/1.5113530

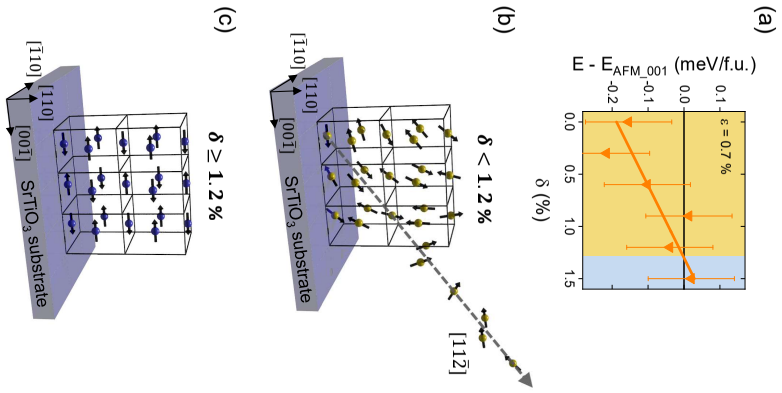


AIP Publishing

Applied Physics Reviews ACCEPTED MANUSCRIPT

This is the author's peer reviewed, accepted manuscript. However, the online version of record will be different from this version once it has been copyedited and typeset.

PLEASE CITE THIS ARTICLE AS DOI: 10.1063/1.5113530



AIP Publishing

Applied Physics Reviews ACCEPTED MANUSCRIPT

This is the author's peer reviewed, accepted manuscript. However, the online version of record will be different from this version once it has been copyedited and typeset.

PLEASE CITE THIS ARTICLE AS DOI: 10.1063/1.5113530

